Supporting Information

Dehydroabietylamine-decorated imino-phenols: Supramolecular gelation and gel phase selective detection of Fe^{3+}, Cu^{2+} and Hg^{2+} ions under different experimental conditions

Subhasis Ghosh, Sumit Ghosh, Nabajyoti Baildya and Kumaresh Ghosh*

Department of Chemistry, University of Kalyani, Kalyani-741235, India.
Email: ghosh_k2003@yahoo.co.in

Table 1S. Results of gelation test for **1-3**.

Solvent	**1**	**2**	**3**
DMSO	S	S	S
DMF	S	S	S
THF	S	S	S
CH_3CN	I	I	I
CH_3OH	I	I	I
Nitrobenzene	S	S	S
$CHCl_3$	S	S	S
Diethyl ether	I	I	I
DCM	S	S	S
Toluene	S	S	S
1,4 Dioxane	S	S	S
1,4-Dioxane: H_2O (4:1 v/v)	**G (18 mg/mL)**	**G (34 mg/mL)**	**G (28 mg/mL)**
DMSO: H_2O (1:1, v/v)	P	P	P
DMF: H_2O (4:1, v/v)	**G (20 mg/mL)**	P	P
DMSO: H_2O (4:1, v/v)	**G (20 mg/mL)**	P	P

G = Gel (mgc); I = Insoluble; P = Precipitation. Gelation was primarily investigated by inversion of vial method after 10-15 mins of sample preparation ([Gelator] = 20 mg/mL).

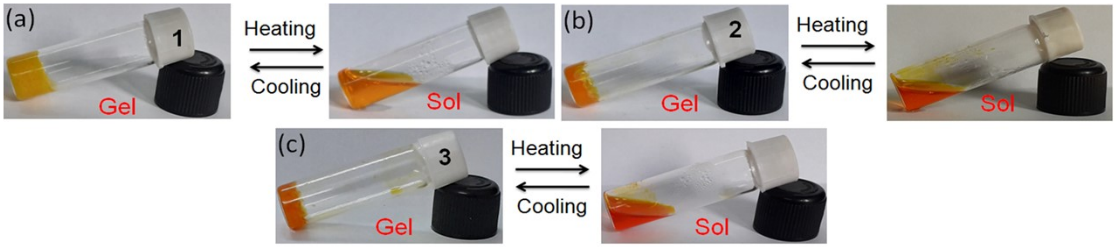

Figure 1S. Pictorial representation of the thermo reversibility of the 1,4 Diox- H_2O (4:1, v/v) gels of **(**a) **1**, (b) **2** and (c) **3**.

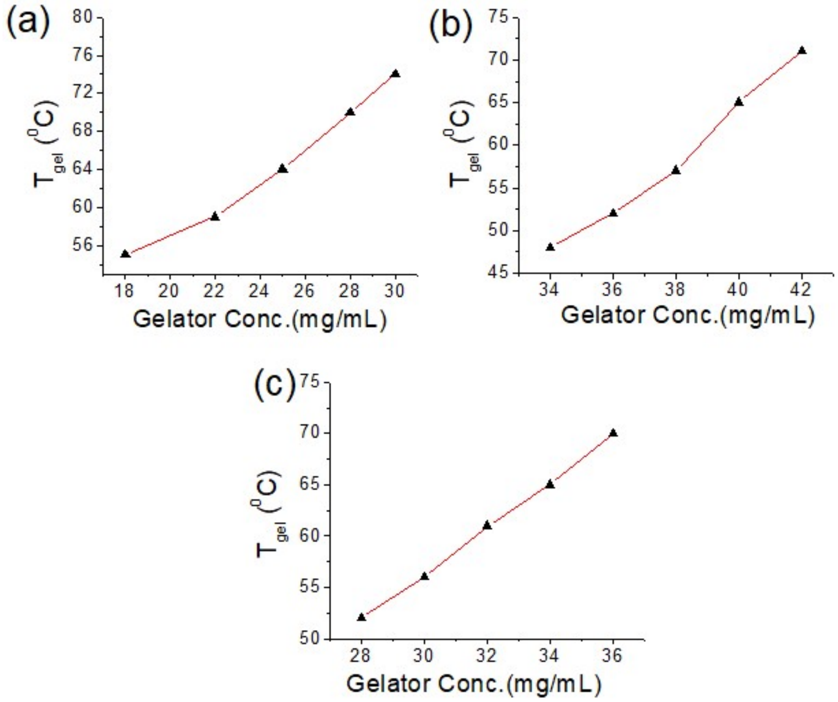

Figure 2S. T_{gel} vs gelators conc. (mg/mL) plots of (a) **1**, (b) **2** and (c) **3**.

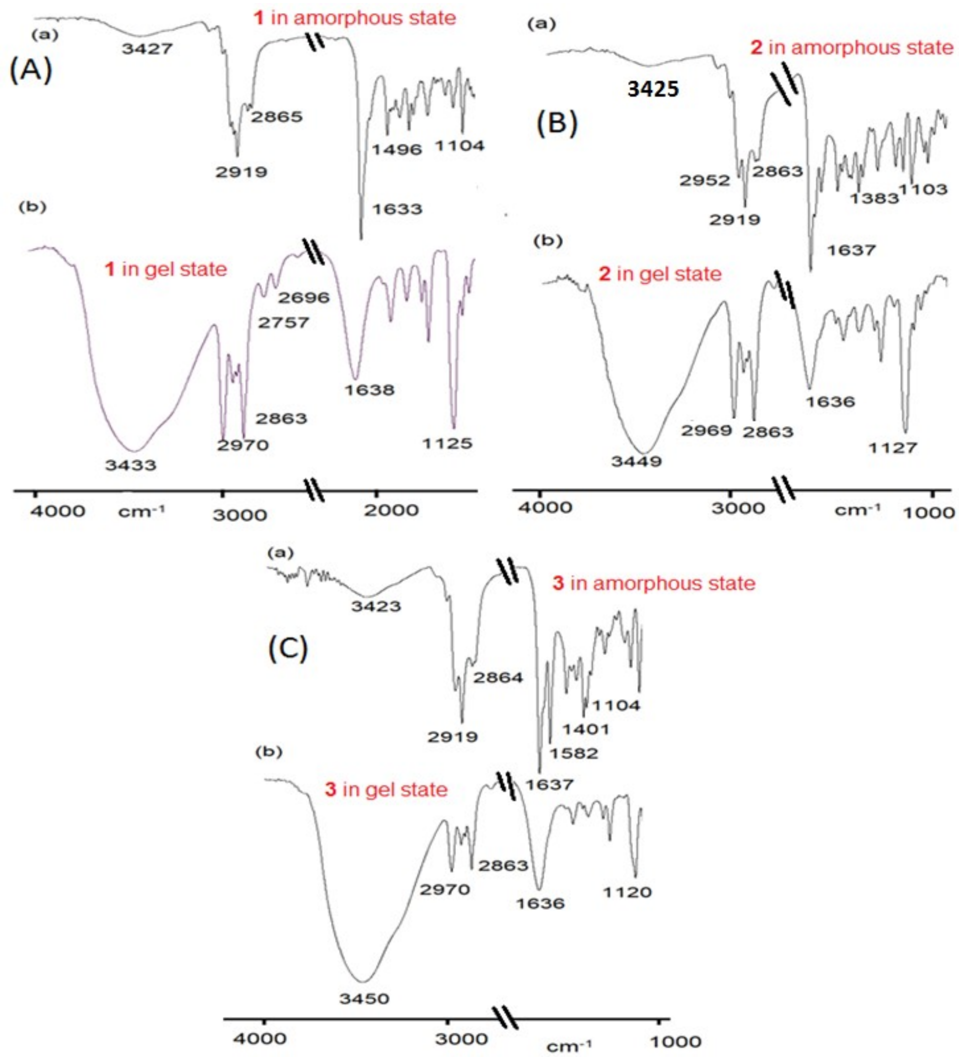

Figure 3S. Partial FTIR spectra of (A) **1** in (a) amorphous and (b) gel state, (B) **2** in (a) amorphous and (b) gel state and (C) **3** in (a) amorphous and (b) gel state.

Table 2S. Major electronic transitions for **1** in aggregated form in 1,4-dioxane-water medium.

Transition No.	**Energy (cm^{-1})**	**Wavelength λ_{max}(nm)**	**Oscillator Strength (f)**	**Major compositions (contribution)**
1	21564.04	463.735	0.0283	H-1→L+1 (19%), H→L (21%), H→L+1 (26%)
2	21944.73	455.6902	0.0261	H→L+1 (18%)
3	21985.06	454.8543	0.0195	H-14→L+3 (20%), H-1→L+2 (17%), H→L+2 (23%)
4	22375.43	446.9187	0.0211	H-14→L+3 (16%), H→L+2 (15%)
5	22400.44	446.4199	0.0028	H-21→L (18%), H-19→L (22%)
6	22700.47	440.5194	0.0041	H-20→L+1 (26%), H-17→L+1 (19%)
7	22923.08	436.2415	0.0216	H→L+3 (19%)
8	22982.77	435.1086	0.0011	H-1→L (18%), H-1→L+1 (38%), H→L+1 (30%)
9	23199.73	431.0395	0.0298	H-1→L+3 (18%), H→L+3 (25%)
10	23280.39	429.5461	0.0003	H-1→L (43%), H-1→L+1 (18%), H→L (27%)
11	23640.92	422.9954	0.0225	H-4→L+1 (30%), H-4→L+2 (24%)
12	23953.05	417.4833	0.0025	H-4→L (26%), H-4→L+2 (19%)
13	24076.46	415.3435	0.0093	H-2→L+1 (54%)
14	24115.98	414.6629	0.0027	H-1→L+2 (41%), H→L+2 (29%)
15	24165.98	413.8048	0.0059	H-3→L (35%)
16	24187.76	413.4322	0.0088	H-3→L (48%)
17	24428.92	409.3509	0.0004	H-2→L (71%), H-2→L+1 (24%)
18	24705.57	404.767	0.0003	H-3→L+1 (92%)
19	24749.93	404.0416	0	H-1→L+3 (52%), H→L+3 (39%)
20	24765.25	403.7915	0.0014	H-2→L+2 (88%)
21	24851.56	402.3893	0.0009	H-7→L+1 (41%), H-4→L+1 (16%)
22	25105.62	398.3172	0.0007	H-2→L+3 (82%)
23	25190.31	396.9781	0.0013	H-9→L+1 (31%), H-6→L+1 (27%)
24	25257.25	395.9259	0.0004	H-9→L+1 (22%), H-6→L (23%), H-6→L+1 (40%)
25	25533.09	391.6486	0.0036	H-6→L (66%), H-6→L+1 (28%)
26	25624.23	390.2556	0.0026	H-5→L (71%)
27	**25690.37**	**389.2509**	**0.0444**	**H-4→L+3 (45%)**
28	25750.06	388.3487	0.0006	H-7→L (32%), H-5→L+1 (38%)
29	25832.33	387.1119	0.0002	H-7→L (16%), H-5→L (15%), H-5→L+1 (54%)
30	25879.91	386.4001	0.0033	H-3→L+2 (84%)

Table 3S. Major electronic transitions for **2** in aggregated form in 1,4-dioxane-water medium.

Transition No.	**Energy (cm^{-1})**	**Wavelength (nm)**	**Oscillator Strength (f)**	**Major contribution**
1	20129.18	496.7913	0.0963	H→L (22%), H→L+2 (17%)
2	20230	494.3154	0.0079	H-6→L (18%)
3	20499.39	487.8195	0.0116	H-13→L (21%)
4	21874.56	457.152	0.0296	H-16→L+1 (29%), H-14→L+1 (44%)
5	22875.5	437.149	0.0613	H→L (70%)
6	23675.6	422.3758	0.0018	H-3→L+1 (25%), H→L+1 (72%)
7	24442.63	409.1212	0.0102	H-2→L (67%), H-1→L (23%)
8	24471.67	408.6358	0.0237	H-3→L (56%)
9	24735.41	404.2787	0.0603	H-3→L+2 (17%), H→L+2 (41%)
10	24811.23	403.0433	0.003	H-2→L (27%), H-1→L (63%)
11	25019.32	399.6911	0.0007	H-2→L+1 (74%), H-1→L+1 (19%)
12	25098.36	398.4324	0.0029	H-3→L+1 (66%), H→L+1 (24%)
13	25213.7	396.6098	0.016	H-6→L (54%)
14	25621.81	390.2924	0.0001	H-2→L+1 (20%), H-1→L+1 (72%)
15	25654.88	389.7893	0.0623	H-3→L+2 (63%), H→L+3 (23%)
16	25740.38	388.4947	0	H-4→L (91%)
17	25843.62	386.9427	0.0006	H-6→L+1 (89%)
18	26317.87	379.9699	0.0975	H-8→L (25%), H-5→L (15%), H→L+3 (24%)
19	26335.62	379.7139	0.0063	H-2→L+2 (32%), H-1→L+2 (59%)
20	26387.23	378.9711	0	H-4→L+1 (93%)
21	26523.54	377.0235	0.0106	H-2→L+2 (53%), H-1→L+2 (36%)
22	26636.46	375.4253	0.0244	H-5→L (71%)
23	**26663.08**	**375.0505**	**0.1096**	**H-6→L+2 (36%)**
24	27136.52	368.507	0.0333	H-11→L (22%), H-8→L+2 (16%)
25	27314.77	366.1023	0.0023	H-5→L+1 (87%)
26	27341.39	365.7459	0.0124	H-11→L+1 (33%), H-8→L+1 (30%)
27	27368.81	365.3794	0.0449	H-4→L+2 (66%)
28	27422.04	364.6701	0.1059	H-4→L+2 (22%), H-3→L+3 (37%)
29	27543.03	363.0683	0.0003	H-10→L (16%), H-9→L (64%)
30	27588.19	362.4739	0.002	H-7→L (33%)

Table 4S. Major electronic transitions for **3** in aggregated form in 1,4-dioxane-water medium.

Transition No.	Energy (cm^{-1})	Wavelength (nm)	Oscillator Strength (f)	Major contribution
1	19430.7	514.6494	0.0065	H→L (36%)
2	19706.54	507.4456	0.0009	H-4→L+2 (15%)
3	19803.33	504.9656	0.0107	H-2→L+2 (17%), H→L (31%)
4	19923.51	501.9197	0.0018	H-16→L+1 (22%)
5	20221.93	494.5126	0.0013	H-20→L (65%)
6	20809.1	480.5589	0.0027	H-1→L (75%)
7	21340.62	468.5899	0.0004	H→L+1 (74%)
8	**22470.61**	**445.0258**	**0.0116**	**H-1→L+1 (65%)**
9	22639.98	441.6964	0.009	H→L+2 (58%)
10	22877.92	437.1027	0.0039	H-2→L (28%)
11	23110.2	432.7093	0.0005	H-7→L (16%), H-6→L (23%), H-2→L (21%)
12	23425.57	426.884	0.001	H-4→L (48%), H-2→L (37%)
13	24203.89	413.1567	0.0001	H-3→L (92%)
14	24489.41	408.3397	0.0014	H-2→L+1 (43%)
15	24720.89	404.5161	0.0057	H-16→L (34%), H-5→L (16%)
16	24762.83	403.831	0.0011	H-5→L (82%)
17	24976.57	400.3752	0.0016	H-4→L+1 (44%)
18	25182.24	397.1052	0.0004	H-7→L (55%), H-6→L (37%)
19	25274.19	395.6606	0.0026	H-10→L (16%), H-1→L+2 (24%), H→L+3 (17%)
20	25391.95	393.8257	0.0104	H-16→L (21%), H-10→L (45%)
21	**25945.24**	**385.4271**	**0.0723**	**H→L+3 (18%)**
22	25990.41	384.7573	0.0001	H-8→L (100%)
23	26252.54	380.9155	0.0003	H-15→L (19%), H-11→L (16%), H-3→L+1 (35%)
24	26292.87	380.3313	0.0002	H-15→L (30%), H-13→L (17%), H-3→L+1 (34%)
25	26454.18	378.0121	0.0001	H-11→L (34%), H-9→L (36%), H-3→L+1 (16%)
26	26496.93	377.4023	0.0117	H-2→L+3 (20%), H-1→L+3 (23%)
27	26566.29	376.4169	0.0017	H-11→L (24%), H-9→L (50%)
28	26614.68	375.7324	0.004	H-6→L+1 (16%)
29	26834.87	372.6494	0.0001	H-12→L (72%), H-11→L (17%)
30	26938.11	371.2213	0.0004	H-5→L+1 (97%)

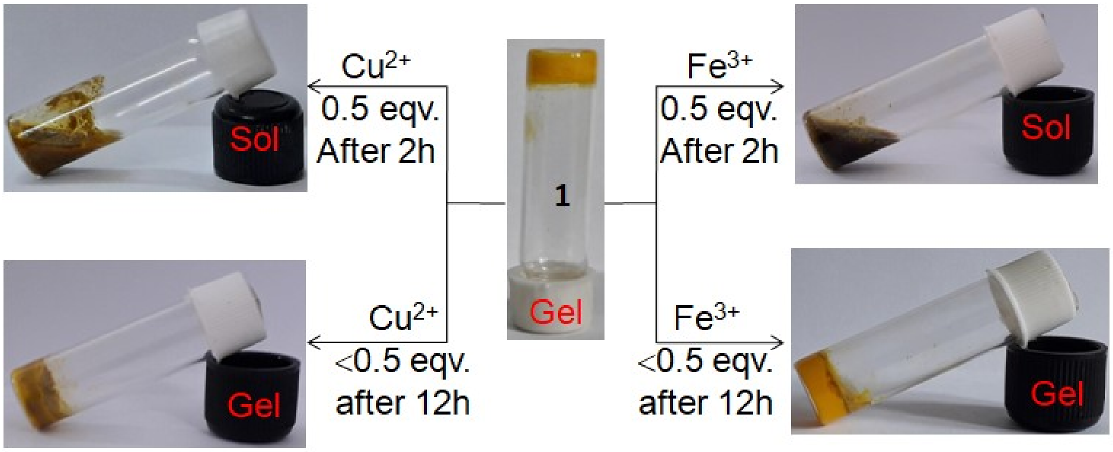

Figure 4S. Picture showing the minimum amounts of metal ions required for gel-to-sol phase transition of 1,4 dioxane-H_2O (4:1, v/v) gel of **1**.

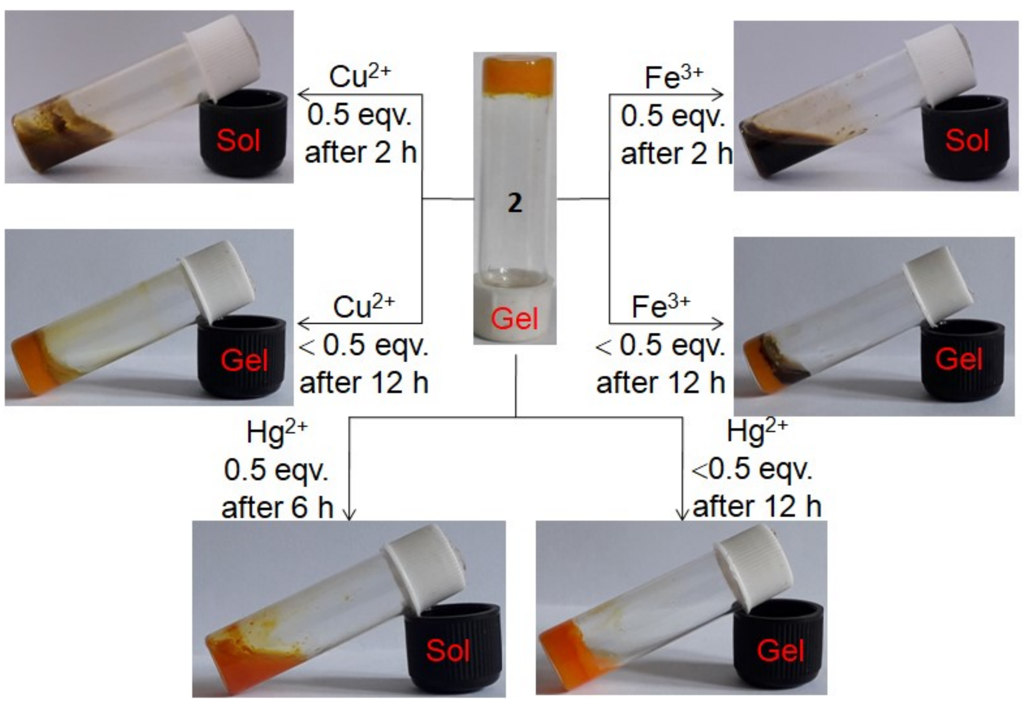

Figure 5S. Picture showing the minimum amounts of metal ions required for gel-to-sol phase transition of 1,4 dioxane-H_2O (4:1, v/v) gel of **2**.

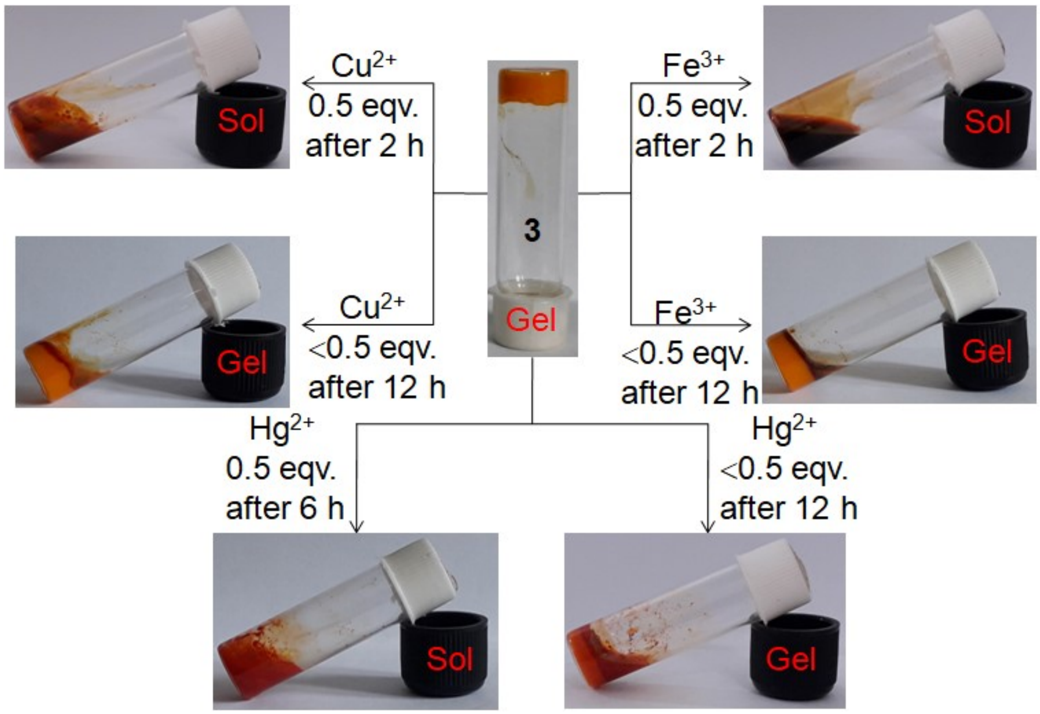

Figure 6S. Picture showing the minimum amounts of metal ions required for gel-to-sol phase transition of 1,4 dioxane-H_2O (4:1, v/v) gel of **3**.

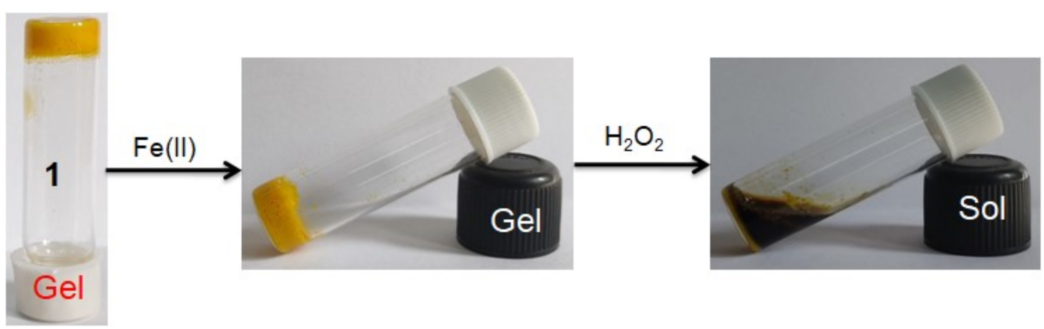

Figure 7S. Chemical responsiveness of the yellow colored 1,4 dioxane-H_2O (4:1, v/v) gel of **1** in different conditions.

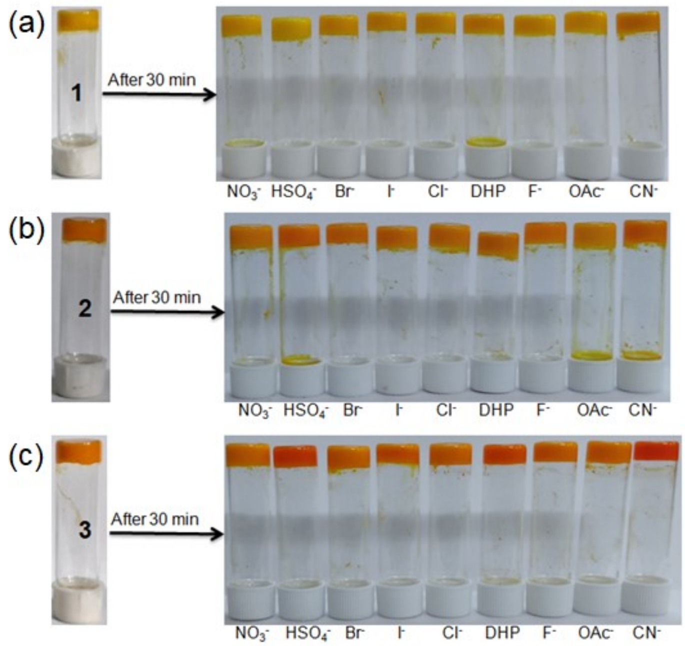

Figure 8S. Photograph showing the phase changes of gels (a) **1**, (b) **2** and (c) **3** in 1,4-dioxane-H_2O (4:1, v/v) in the presence of equiv. amount of different anions after 30 mins [at mgc; all were used as tetrautylamonium salts].

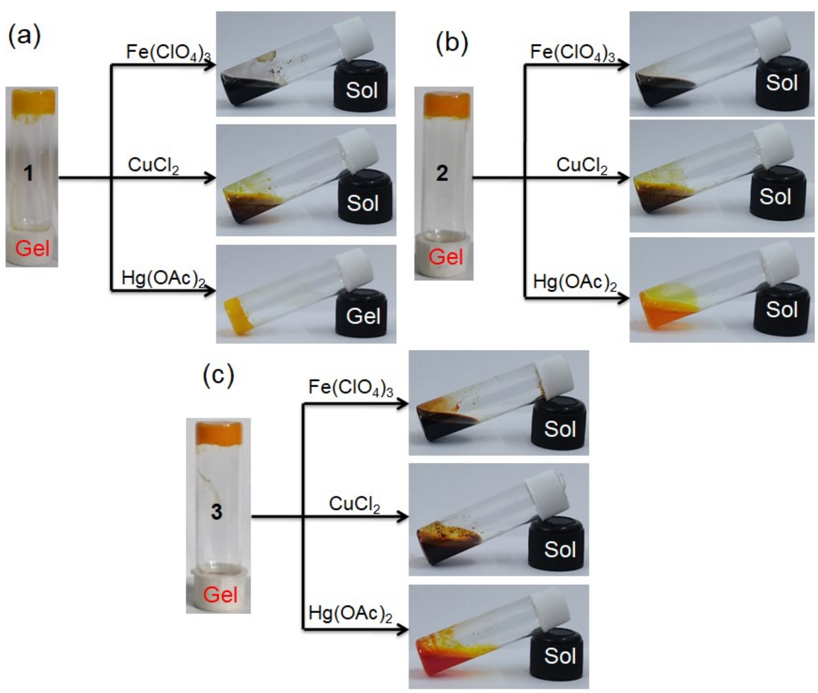

Figure 9S. Photograph showing the phase changes of gels (a) **1**, (b) **2** and (c) **3** in 1,4-dioxane-H_2O (4:1, v/v) in the presence of equiv. amount of different anionic salt of $Cu^{2+,}$ Fe^{3+} and Hg^{2+} after 30 mins.

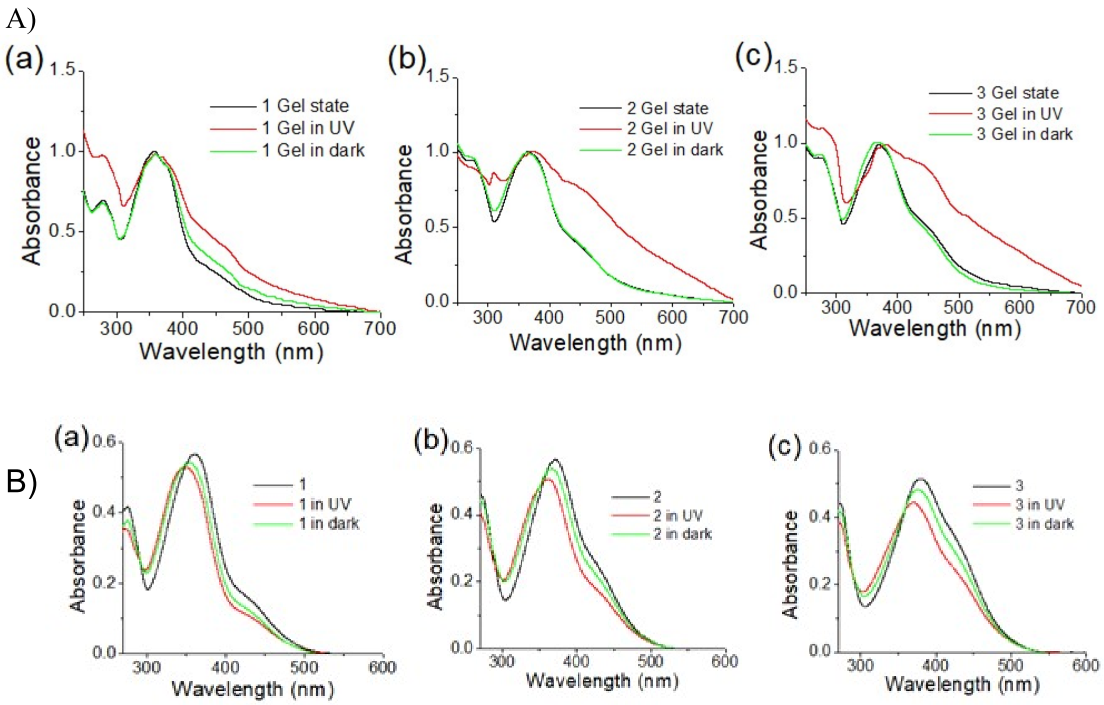

Figure 10S. UV-vis study for the isomerisation of (A) gels (a) **1**,(b) **2** and (c) **3** in 1,4-Dioxane-H_2O (4:1, v/v) and (B) solutions of (a) **1**, (b) **2** and (c) **3** (c = 2.5 x 10^{-5} M) in 1,4-Dioxane-H_2O (4:1, v/v) upon exposure to 390 nm UV light. UV light was exposed on the samples for 1 hour.

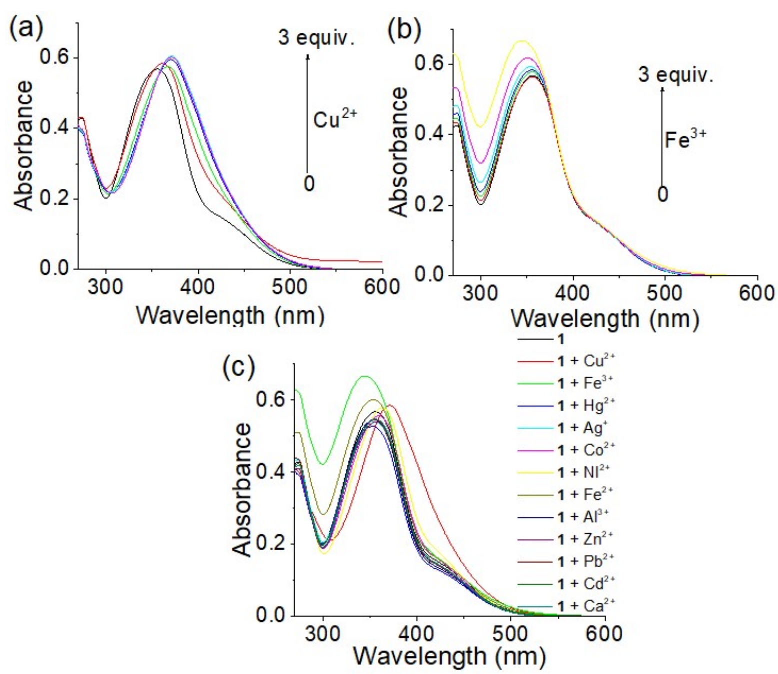

Figure 11S. Change in absorbance of **1** (c = 2.5 x 10^{-5} M) upon addition of 3 equiv. amounts of (a) Cu^{2+}, (b) Fe^{3+} and (c) all metals (c = 1.0 x 10^{-3} M) in 1,4-dioxane-H_2O (4:1, v/v).

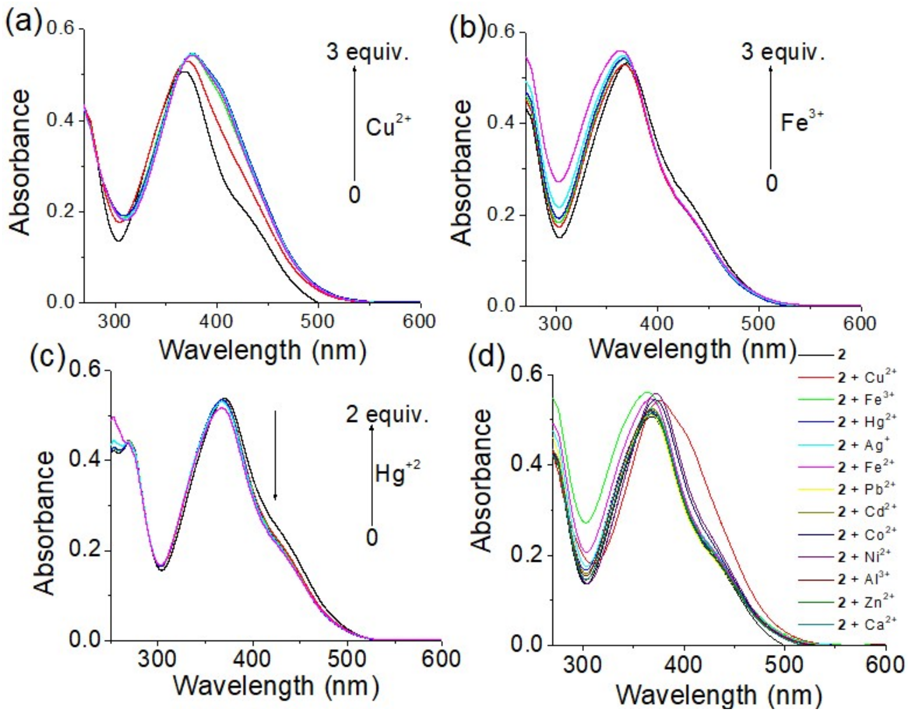

Figure 12S. Change in absorbance of **2** (c = 2.5 x 10^{-5} M) upon addition of 3 equiv. amounts of (a) Cu^{2+}, (b) Fe^{3+}, (c) Hg^{+2} and (d) all metals (c = 1.0 x 10^{-3} M) in 1,4-dioxane-H_2O (4:1, v/v).

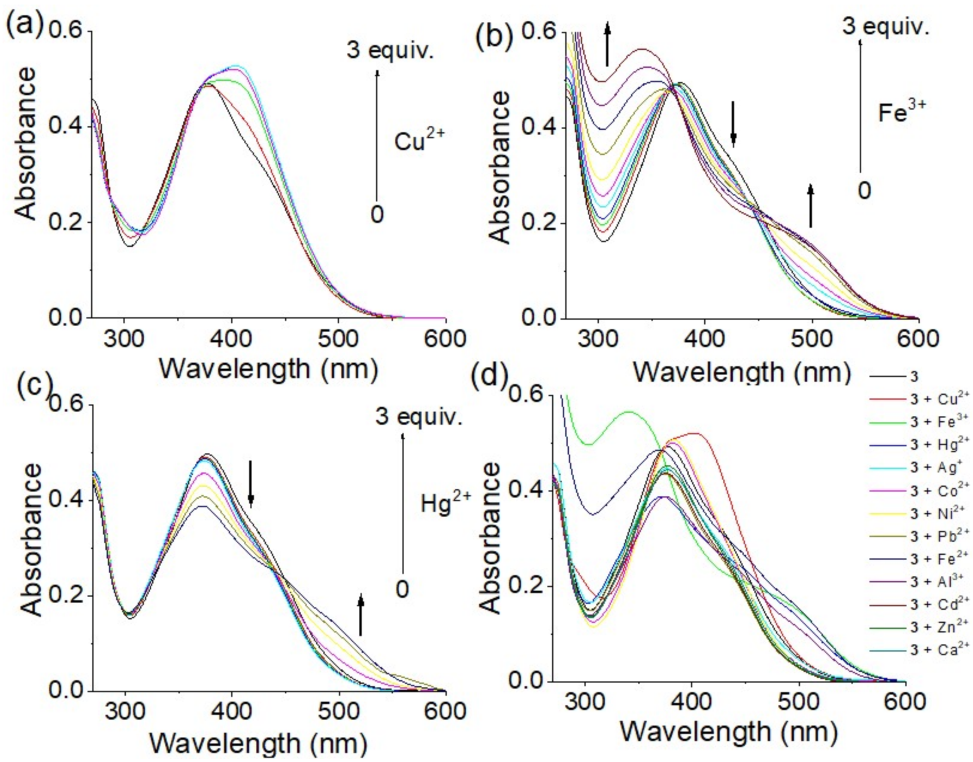

Figure 13S. Change in absorbance of **3** (c = 2.5 x 10^{-5} M) upon addition of 3 equiv. amounts of (a) Cu^{2+}, (b) Fe^{3+}, (c) Hg^{2+} and (d) all metals (c = 1.0 x 10^{-3} M) in 1,4-dioxane-H_2O (4:1, v/v).

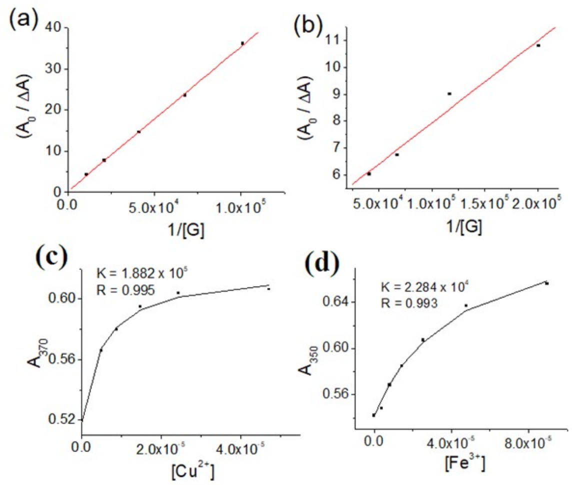

Figure 14S. Benesi–Hildebrand plots for **1** (c = 2.5 x 10^{-5} M) with (a) Fe^{3+} at 350 nm and (b) Cu^{2+} at 370 nm (c = 1.0 x 10^{-3}M) in 1,4-dioxane: H_2O (4:1, v/v) from UV-vis titration. Non liner binding constant curves for **1** (c = 2.5 x 10^{-5} M) with (c) Cu^{2+} and (d) Fe^{3+} .

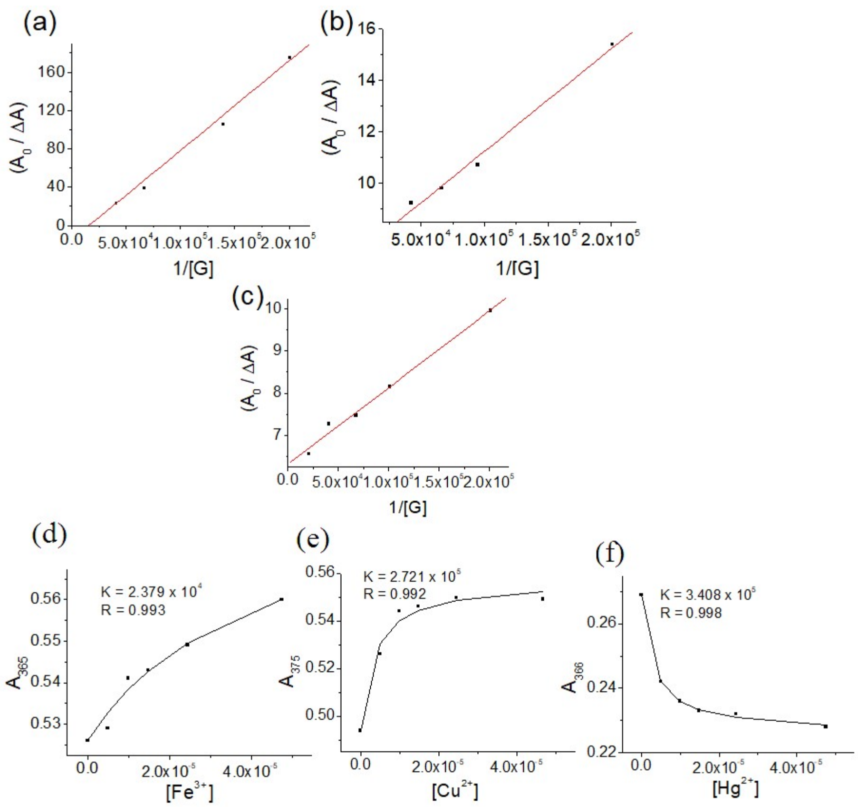

Figure 15S. Benesi–Hildebrand plots for **2** (c = 2.5 x 10^{-5} M) with (a) Fe^{3+} at 365 nm, (b) Cu^{2+} at 375 nm and (c) Hg^{2+},at 424 nm (c = 1.0 x 10^{-3}M) in 1,4-dioxane: H_2O (4:1, v/v) from UV-vis titration. Non liner binding constant curves for **2** (c = 2.5 x 10^{-5} M) with (d) Fe^{3+}, (e) Cu^{2+} and (f) Hg^{2+}.

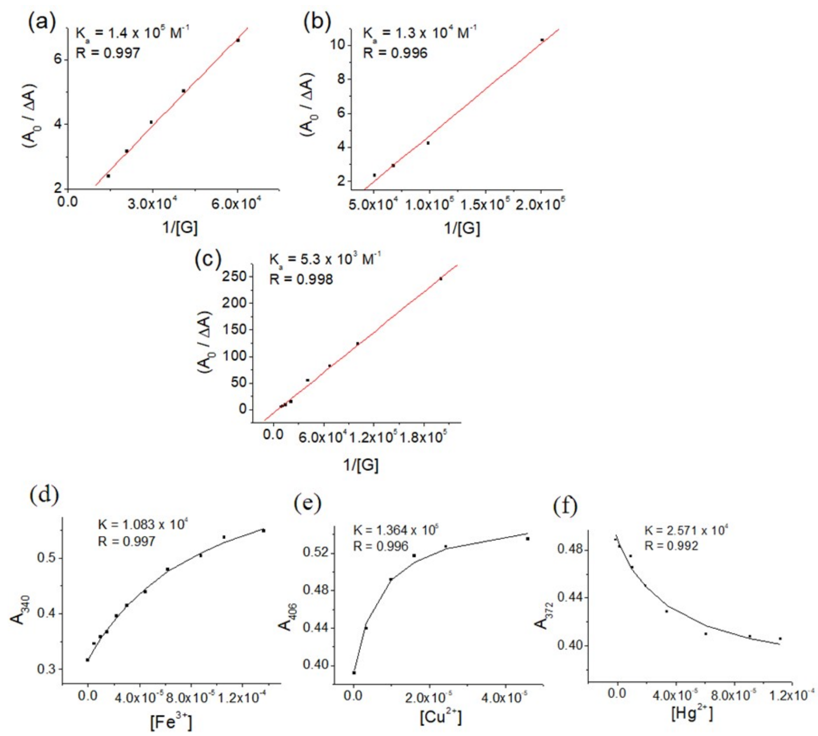

Figure 16S. Benesi–Hildebrand plots for **3** (c = 2.5 x 10^{-5} M) with (a) Fe^{3+} at 340 nm, (b) Cu^{2+} at 406 nm and (c) Hg^{2+}, at 372 nm (c = 1.0 x 10^{-3}M) in 1,4-dioxane : H_2O (4:1, v/v) from UV-vis titration. Non liner binding constant curves for **3** (c = 2.5 x 10^{-5} M) with (d) Fe^{3+} , (b) Cu^{2+} and (c) Hg^{2+} .

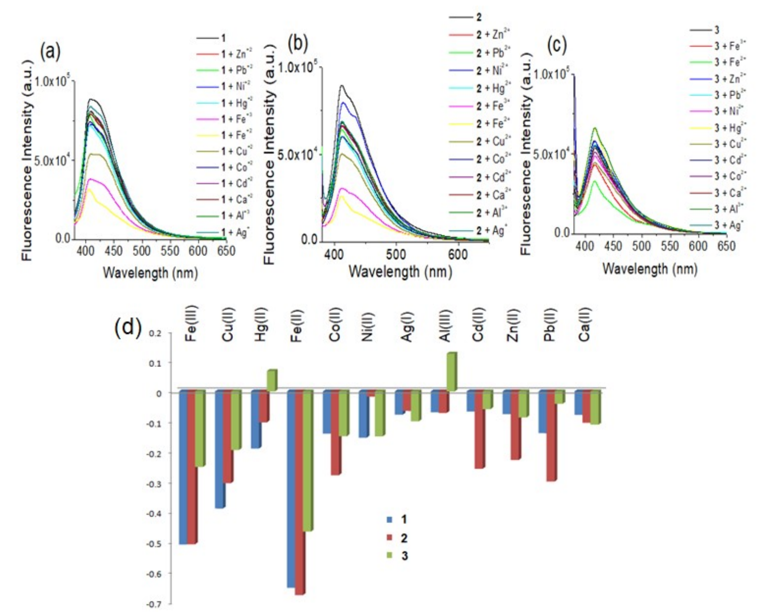

Figure 17S. Change in emission of (a) **1** (λ_{exc} = 370 nm), (b) **2** (λ_{exc} = 370 nm), (c) **3** (λ_{exc} = 370 nm) and (d) Change in fluorescence ratio (λ_{ex} = 370 nm) of **1**, **2** and **3** (c = 2.5 x 10^{-5} M) upon addition of 3 equiv. amounts of different metal ions (c = 1.0 x 10^{-3} M) in 1,4-dioxane-H_2O (4:1, v/v).

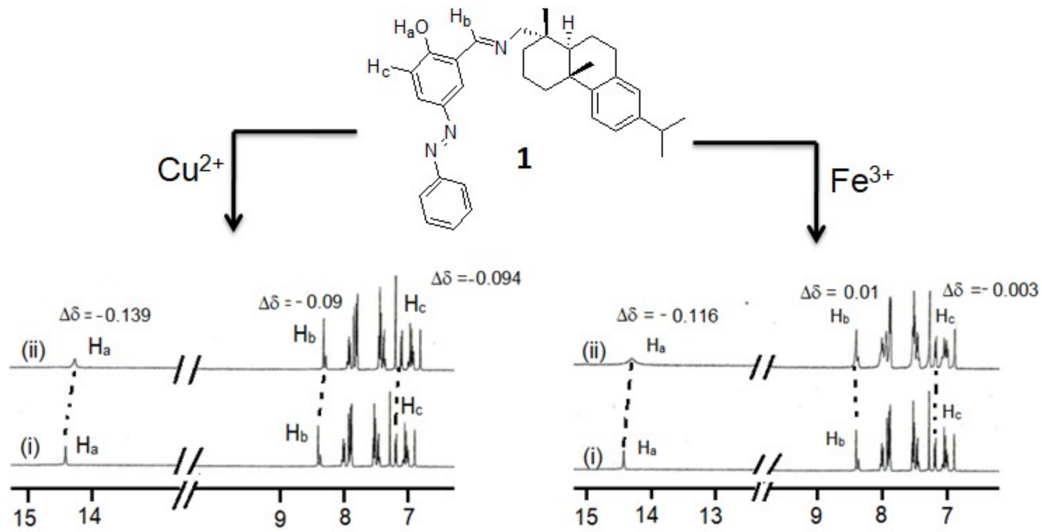

Figure 18S. Partial ^{1}H NMR (400 MHz) of **1** with equivalent amount of Cu^{2+} and Fe^{3+} in $CDCl_3$.

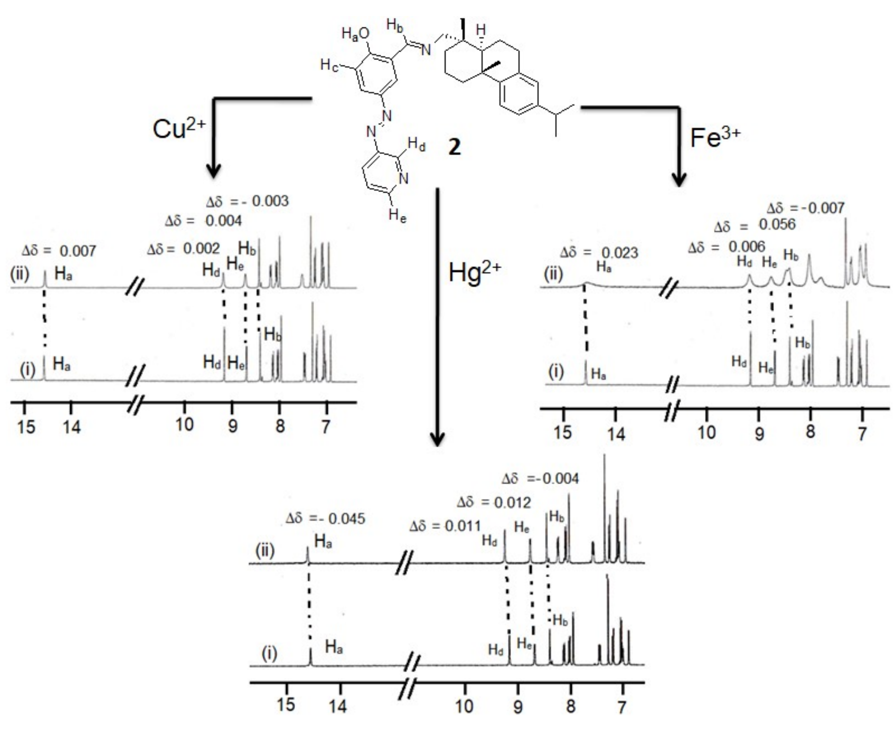

Figure 19S. Partial ^{1}H NMR (400 MHz) of **2** with equivalent amount of Cu^{2+} , Fe^{3+} and Hg^{2+} in $CDCl_3$.

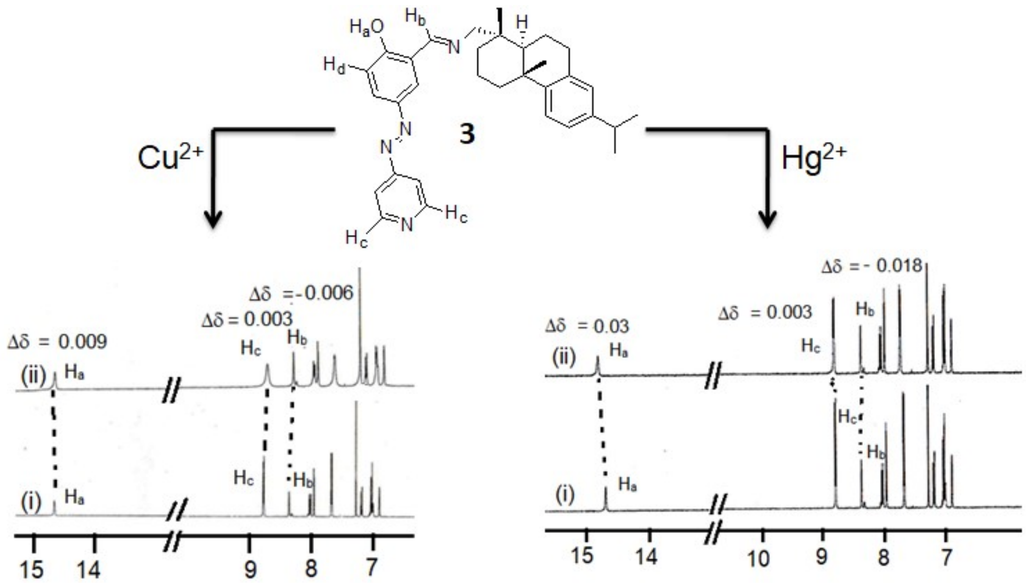

Figure 20S. Partial ^{1}H NMR (400 MHz) of **3** with equivalent amount of Cu^{2+} and Hg^{2+} in $CDCl_3$**.**

Table 5S. Reported gelators based on imino-phenol motif in gel-phase sensing of metal ions.

Sl. No.	structure	Detection	solvent	Interference	Ref.
01	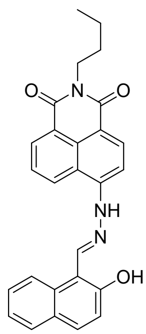	Visual detection through Gel-to Sol transition	DMF: H_2O (1:1, v/v)	Fe^{3+}	1
02	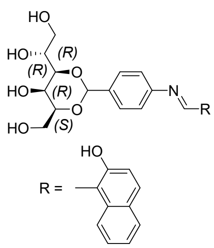	Visual detection through Gel-to Sol transition	DMSO/H_2O (1:1, v/v)	Cu^{2+}	2
03	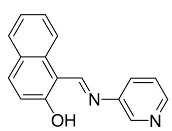	Visual detection through Gel-to Gel transition	DMSO/H_2O (1:1, v/v)	Fe^{3+}	3
04	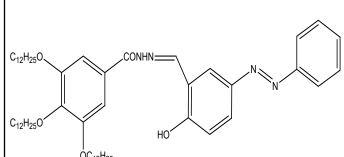	Visual detection through Gel-to Sol transition	DMF	CN^-, F^-, AcO^- and $H_2PO_4^-$	4
05	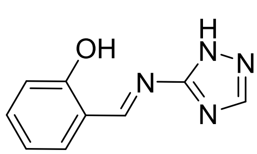	Visual detection through Gel-to Sol transition	DCM	F^- and Ca^{2+}, Zn^{2+}, Mn^{2+}, Fe^{3+}, Cu^{2+}, Co^{2+} and Ni^{2+}	5

06	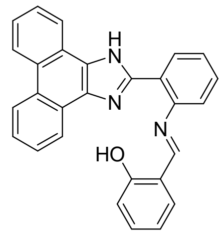		DMF/H_2O (1:1,v/v)	Cu^{2+}	6
07	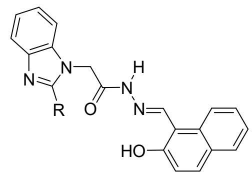 (R = hexyl)	Visual detection through Gel-to Solution transition	Ethylene glycol	Al^{3+}	7
This work	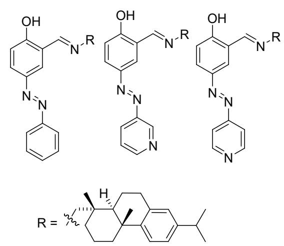	Visual detection through Gel-to Sol transition	1,4-dioxane-H_2O (4:1, v/v)	Fe^{3+}, Cu^{2+} and Hg^{2+} with good sensitivity	-

^1H NMR ($CDCl_3$, 400 MHz) of 1

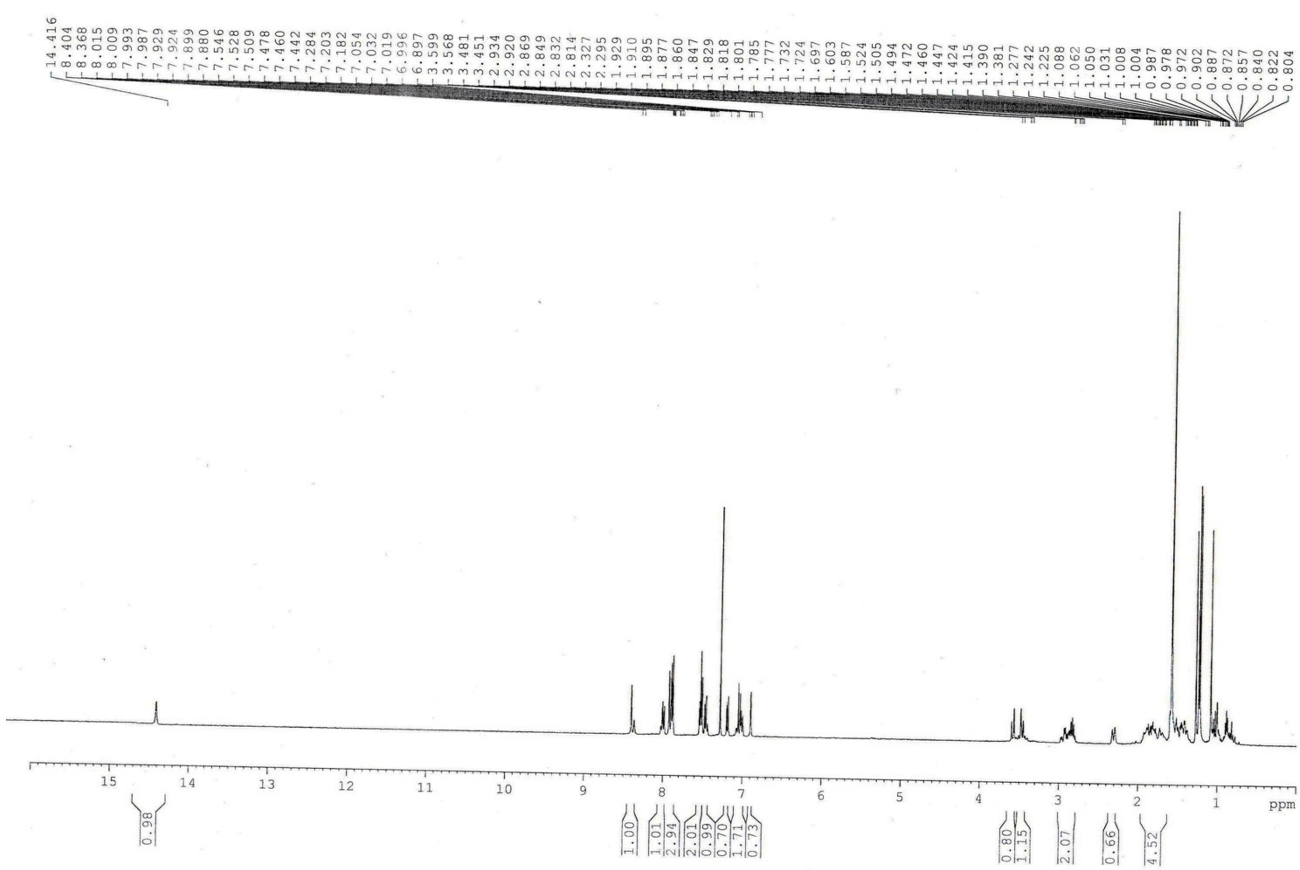

^{13}C NMR (CDCl$_3$, 100 MHz) of 1

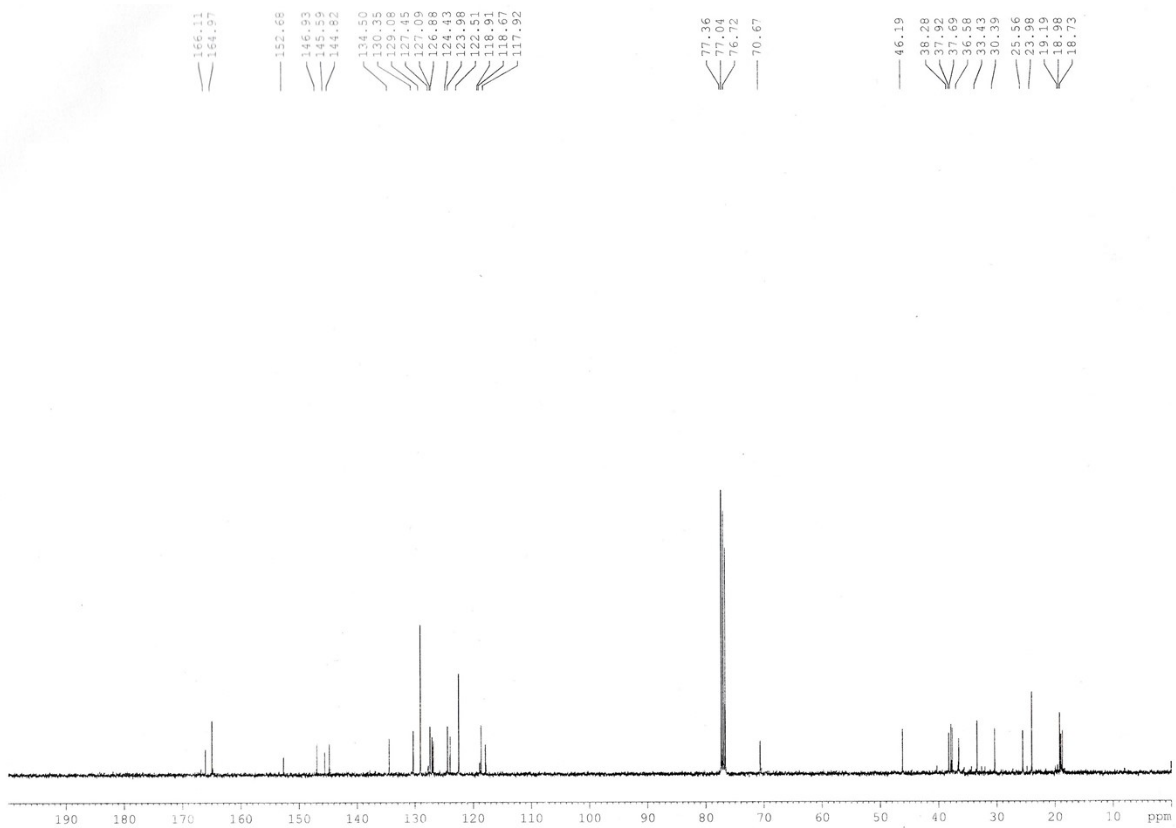

Mass spectrum of 1.

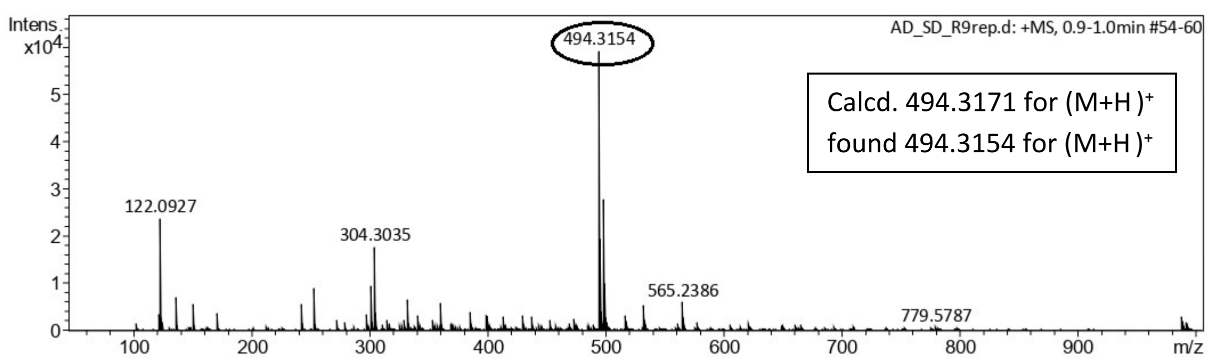

^{1}H NMR ($CDCl_3$, 400 MHz) of 2

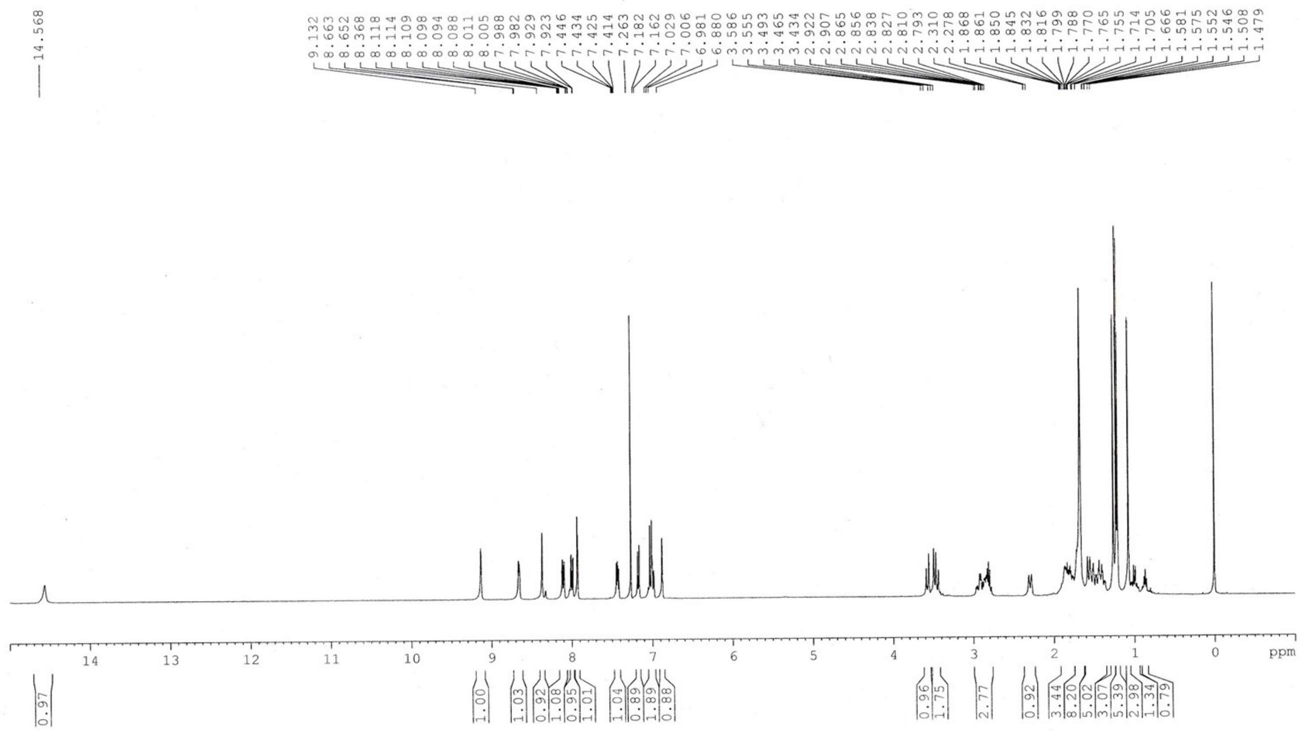

^{13}C NMR ($CDCl_3$, 100 MHz) of 2

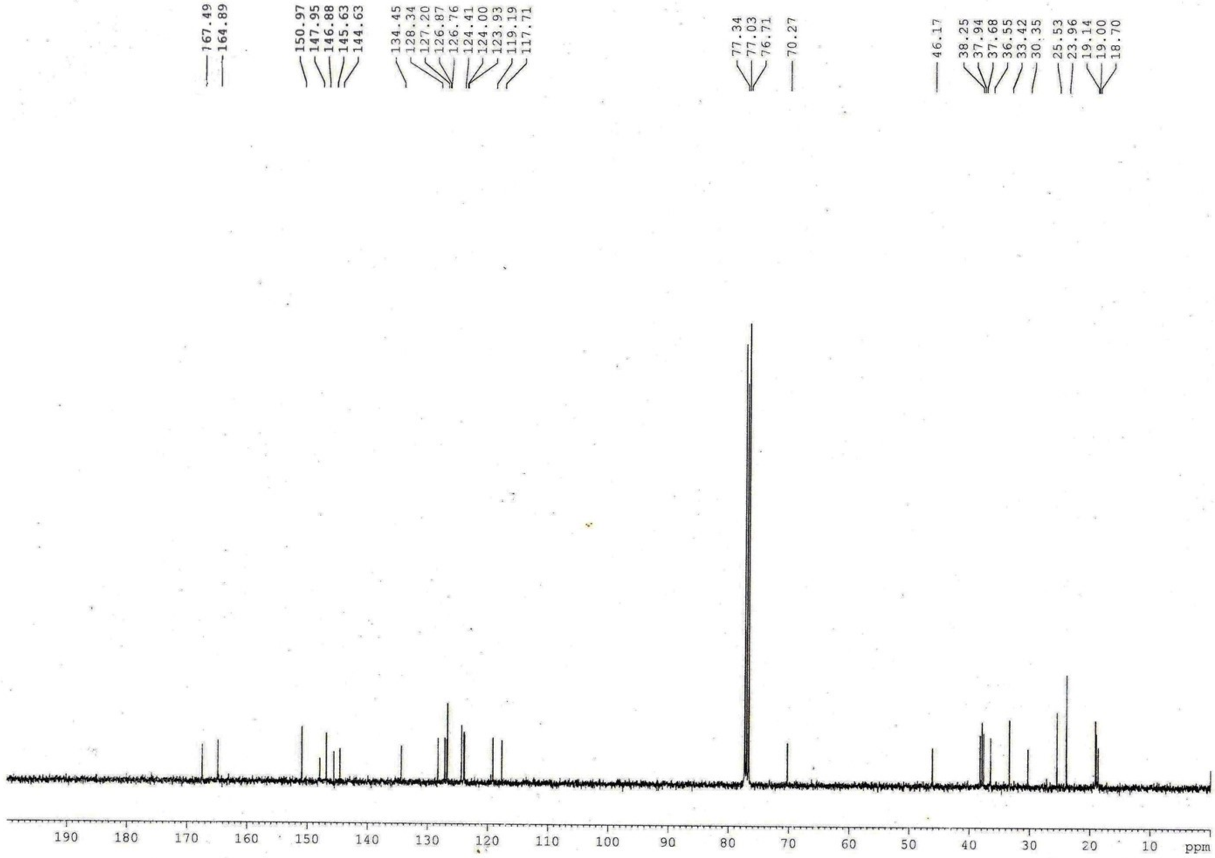

Mass spectrum of 2.

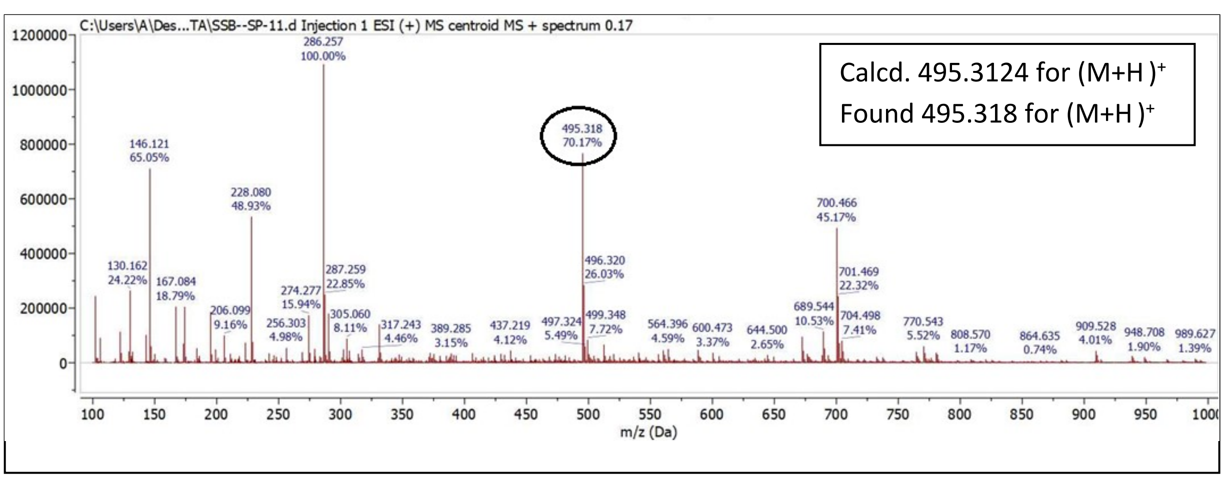

[1]H NMR ($CDCl_3$, 400 MHz) of 3

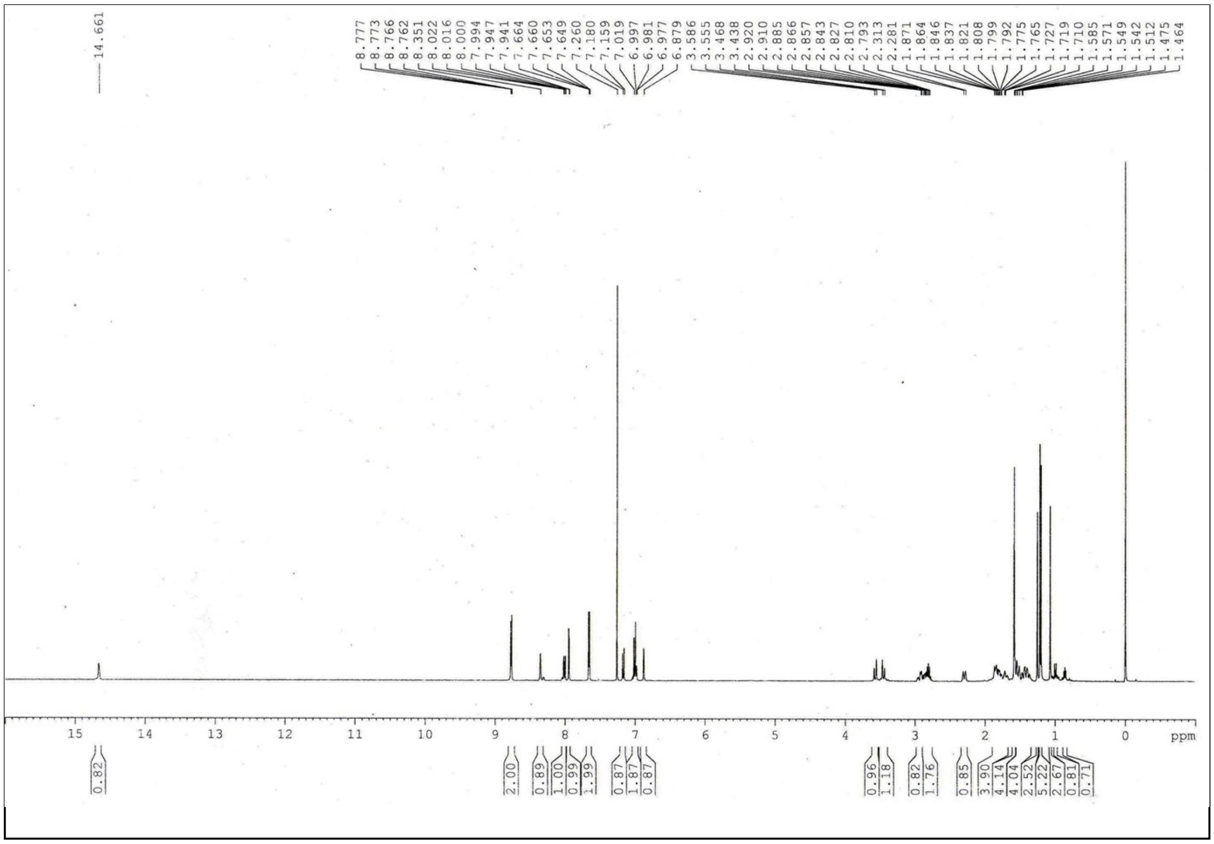

[13]C NMR ($CDCl_3$, 100 MHz) of 3

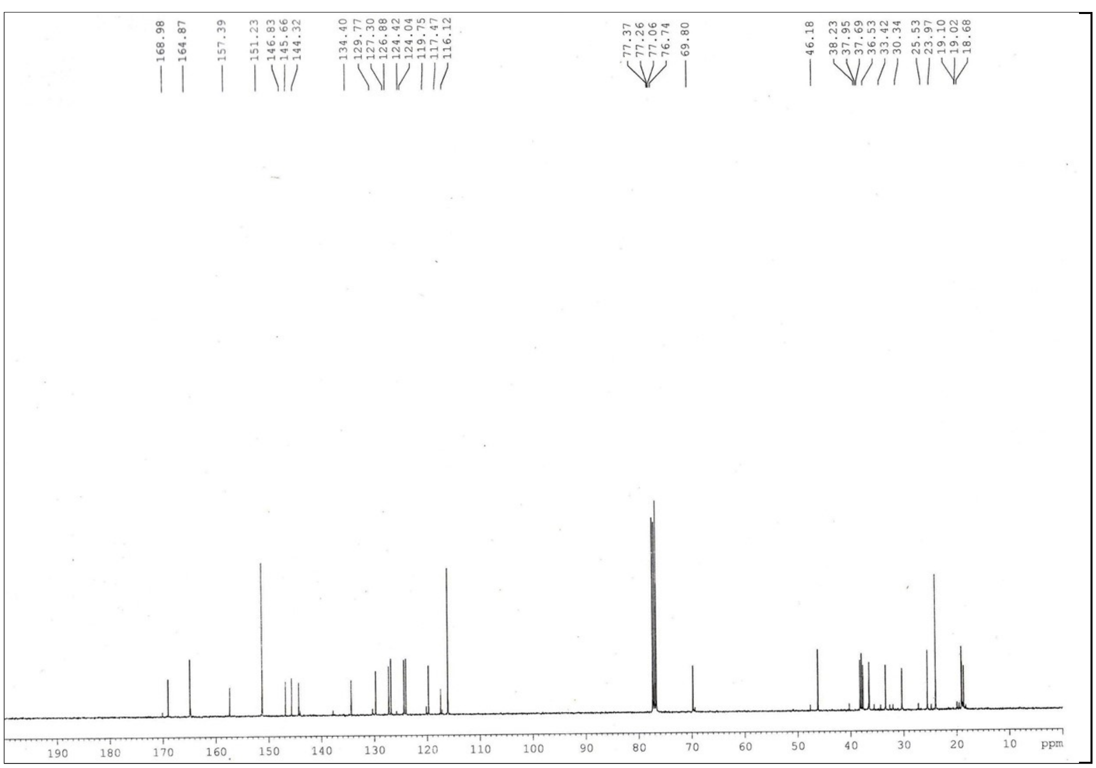

Mass spectrum of 3

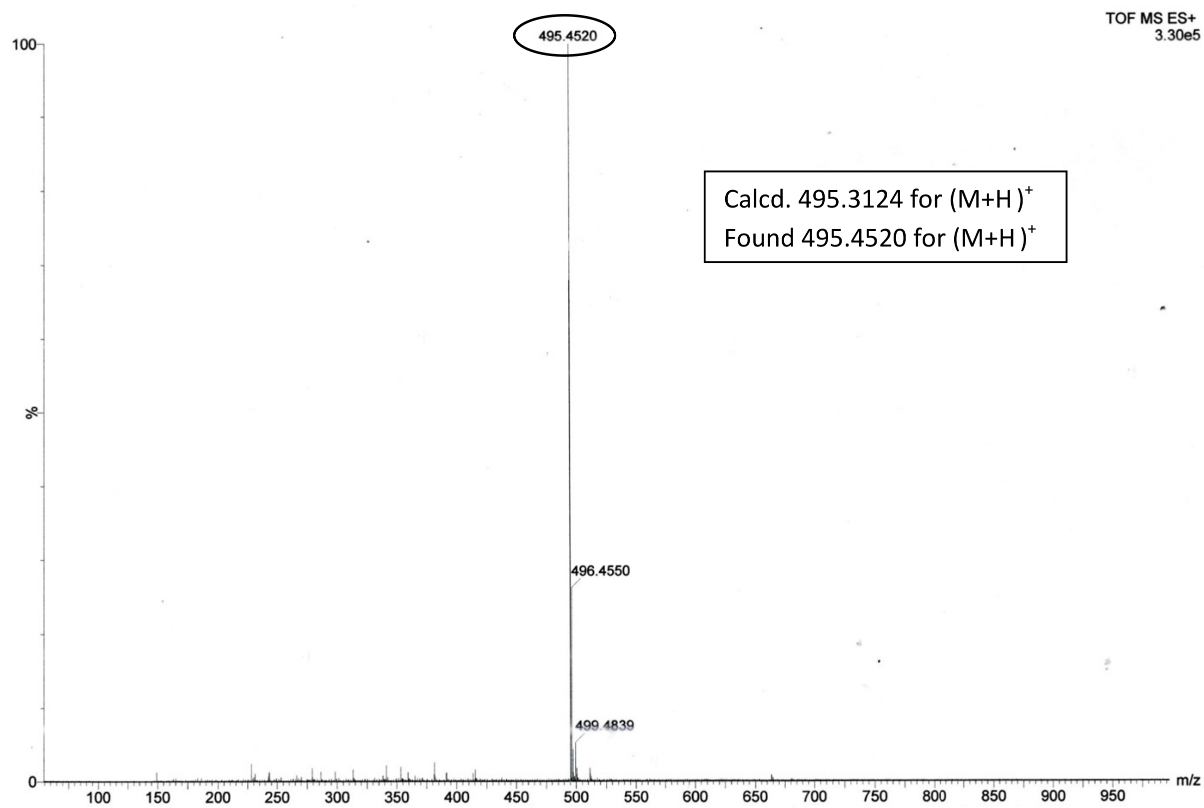

^{1}H NMR ($CDCl_3$, 400 MHz) of 4

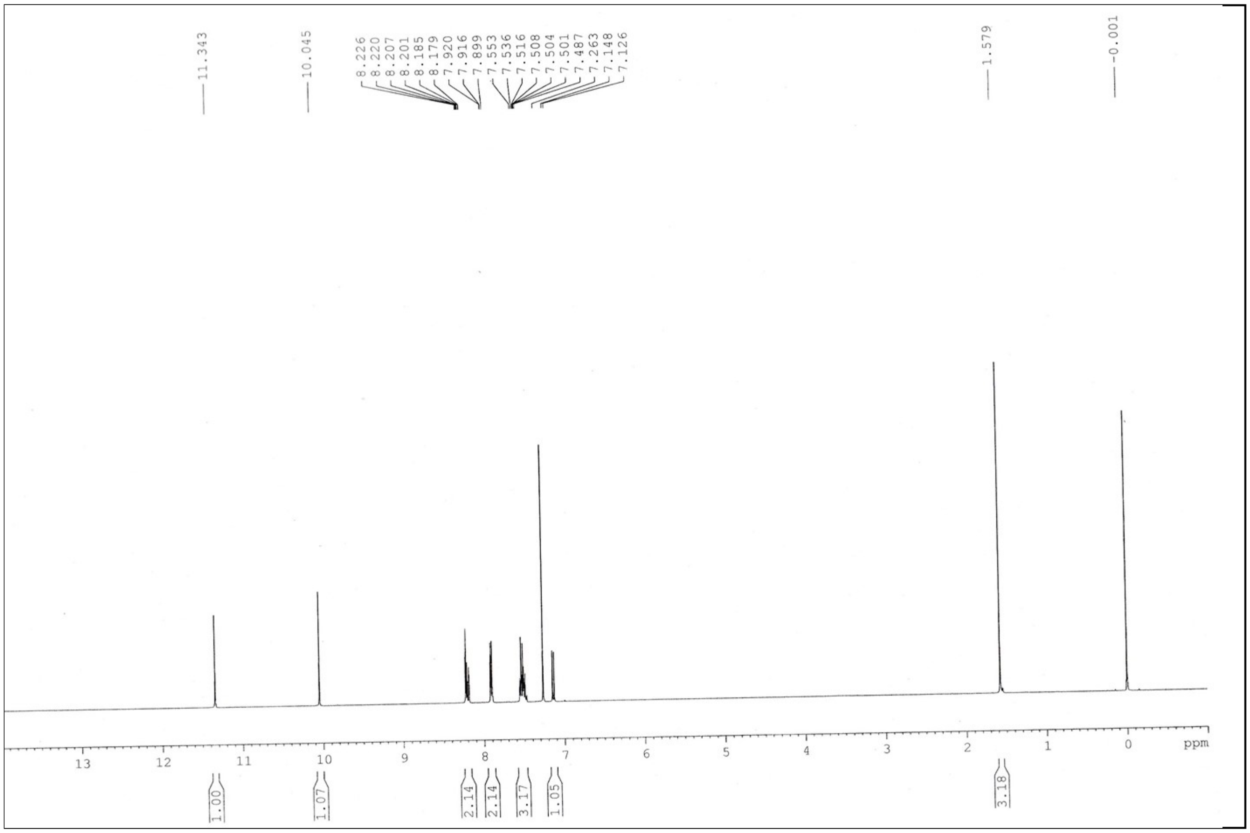

^{1}H NMR ($CDCl_3$, 400 MHz) of 6

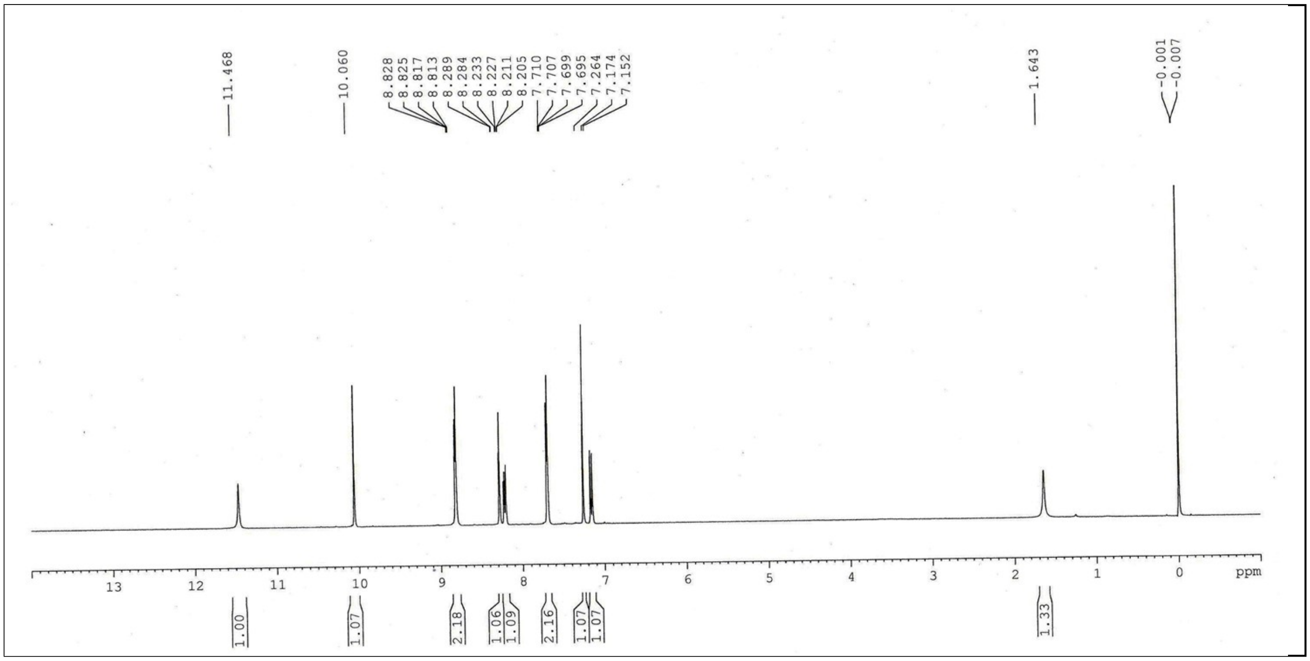

Reference

1. S. Ghosh, N. Baildya, N. N. Ghosh and K. Ghosh, *New Journal of Chemistry*, 2021, **45**, 5213-5220.

2. K. Fan, J. Song, J. Li, X. Guan, N. Tao, C. Tong, H. Shen and L. Niu, *Journal of Materials Chemistry C*, 2013, **1**, 7479-7482.

3. A. Panja and K. Ghosh, *Materials Chemistry Frontiers*, 2018, **2**, 1866-1875.

4. W. Chen, W. Gong, J. Ye, Y. Lin and G. Ning, *RSC Advances*, 2012, **2**, 809-811.

5. Y. Wang, J. Xiong, F. Peng, Q. Li and M.-H. Zeng, *Colloids and Surfaces A: Physicochemical and Engineering Aspects*, 2022, **640**, 128445.

6. H. Yin, B. Zhao, W. Kan, T. Liu, W. Wang, G. Yin, L. Wang, Y. Gao and J. Wang, *Spectrochimica Acta Part A: Molecular and Biomolecular Spectroscopy*, 2019, **217**, 18-26.

7. J. Xie, C. Chen, X. Ma and J. Wu, *Inorganic Chemistry Communications*, 2016, **65**, 41-44.